Chemical Engineering Journal 421 (2021) 129765

Contents lists available at ScienceDirect

Chemical Engineering Journal

journal homepage: www.elsevier.com/locate/cej

# Electrochemically-assisted removal of cadmium ions by redox active Cu-based metal-organic framework

Yonghwan Kim [a], Kwiyong Kim [b], Ho Hyeon Eom [a], Xiao Su [b,*], Jae W. Lee [a,*]

[a] Department of Chemical and Biomolecular Engineering, Korea Advanced Institute of Science and Technology (KAIST), Daejeon 305-701, Republic of Korea
[b] Department of Chemical and Biomolecular Engineering, University of Illinois at Urbana-Champaign, Urbana, IL 61801, United States

ARTICLE INFO

*Keywords:*
Electrosorption
Stripping
Metal-organic framework
Redox reaction
Cadmium removal

ABSTRACT

An electrochemically-assisted wastewater treatment using Faradaic materials offers a promising technique for the selective removal of hazardous substances. Here, we demonstrate the reversible capture and release of cadmium ions in aqueous solutions, using a redox-active metal-organic framework (MOF) electrode. As-synthesized copper-based MOF (Cu-MOF-74; copper 2,5-dihydroxyterephthalate) is a highly attractive candidate for Faradaic electrosorption due to its large surface area, water stability, and redox-active metal nodes. Our work demonstrates the reversible capture and release of $Cd^{2+}$ ions assisted by the electrochemical redox reaction of $Cu^{2+}/Cu^{+}$ within the MOF structure. Combined material characterization and electrosorption tests were carried out to determine the operational conditions for maximizing adsorption capacity, energy efficiency, and material stability, thus leading to excellent electrosorption (>100 mg $g^{-1}$) and regeneration efficiency (>90%). This study demonstrates the feasibility of leveraging MOFs containing redox-active metal nodes for the selective separation of toxic cations, and paves the way for promising future applications of these 3-D porous structures for wastewater treatment and environmental remediation.

## 1. Introduction

Securing clean water is an overarching scientific and engineering challenge for improving quality of life worldwide, especially due to accelerated population growth and urbanization [1]. In addition, high-tech industries often necessitate high purity water for processing, while at the same time, wastewater generated by industrialization is increasing at a rapid pace [2,3]. Thus, large volumes of industrial wastewater must be properly treated, especially for prevalent heavy metals that can cause significant damage to human bodies and ecosystems [4,5]. In particular, cadmium (Cd) is a representative hazardous heavy metal that could be released from mining or electronic industrial sites due to its high mobility [6]. It requires proper management, as it has high mobility and perseveres in the human body and can cause fatal damage to the kidney and bones [7,8]. Accordingly, the US Environmental Protection Agency (EPA) has set a strict level of cadmium dissolved in drinking water of below 5 μg $L^{-1}$ [9]. Cadmium, along with other industrially-relevant heavy metals, has been treated by several methods such as coagulation/flocculation [10,11] or membrane processes [12–16], with adsorption being a highly attractive method due to its selectivity [17–21].

While selective adsorption for $Cd^{2+}$ enables cost-effective separation from wastewater with a large number of competing cations, especially sodium ions [22,23], a strong acid or a high concentration of salt is often required for the reuse and regeneration of the adsorbents. This process can often damage the adsorbent material, thus decreasing the performance, while generating significant secondary pollution that must then also be treated [24,25]. To solve this problem, electrosorption-based methods recently have been gaining attention as a sustainable pathway for heavy metal treatment [26–29]. By regenerating the adsorbent material through electrochemical potential, it removes the need for extensive chemical input [30].

Electrosorption technologies have made rapid progress in a number of desalination applications, including capacitive deionization systems with membrane assistance [31–34] and flow-electrode configurations [34–37]. More recently, tuning the electrosorption process by controlling a Faradaic reaction has given a new dimension to the field, especially through the introduction of redox-active materials [2,38–40]. Using the redox potential of the active material, the generated Faradaic current results in not only enhanced energy efficiency, but also higher adsorption capacity compared to EDLCs [40,41]. In addition, it has been demonstrated in recent studies that redox-induced changes in structure

* Corresponding authors.
*E-mail addresses:* x2su@illinois.edu (X. Su), jaewlee@kaist.ac.kr (J.W. Lee).

https://doi.org/10.1016/j.cej.2021.129765
Received 9 February 2021; Received in revised form 4 April 2021; Accepted 7 April 2021
Available online 16 April 2021

or functional groups can enhance interactions with specific substances in wastewater [24,42–44]. Thus, given the potential of Faradaic processes for tuning both selectivity and potential, the discovery and development of new redox materials is essential for addressing highly diluted target heavy metal ions in wastewater.

Metal-organic frameworks (MOFs), crystalline materials composed of metal nodes and organic linkers, are a promising class of materials for gas and ion adsorption processes in addition to catalysts and sensors, due to their large specific surface area and processability in organic linkers [45–48]. Moreover, water-stable and electrically-conductive MOFs have been recently developed, with a myriad of interesting applications [49–51]. In particular, when a transition metal having various oxidation states exists as a metal node, it could improve conductivity and serve as a redox-active center. Although redox-active MOFs have remarkable potential as Faradaic materials for the electro-sorption system, there are limited cases in which they were used for cation removal [52,53]. An example is that iron(III) of Prussian blue analogues (PBAs) acts as a redox-active center and selectively removes cations such as cesium and calcium [54,55]. HKUST-1, which has copper(II) as a metal center, has also been used as an electrode material for the selective capture of lithium ions [56]. As in these cases, effective removal of cationic target materials is feasible through inducing a reduction of metal nodes by negative overpotential, but not many MOFs have been used for cadmium removal. Therefore, a study on the electrosorption of cadmium using the redox-activity of MOF, which has a high oxidation number of transition metals, is an attractive strategy.

Here, we demonstrate a selective removal of cadmium ions in wastewater using Cu-based MOF-74 as an active material. MOF-74 could be composed of various metal nodes (Zn, Mg, Co, etc.) with a combination of 2,5-dihydroxyterephthalic acid ($H_2$dobdc) [57,58]. Since it has a honeycomb-like structure and a large specific surface area, it is widely used in a broad range of fields such as gas storage [59]. Among various candidate metal sources, Cu-MOF-74 can be expected as a stable redox-active material after redox changes, since Cu is one of the representative transition metals that can exist in divalent, monovalent, or zero-valent forms. Utilizing the MOF crystal in which most of the copper exists in divalent form in the cathodic process was aimed at inducing facile conversion between $Cu^{2+}$ and $Cu^{+}$ to achieve stable adsorption and desorption of cadmium cations (Scheme 1). Therefore, we investigated the change of $Cd^{2+}$ uptake and regeneration efficiency by electrochemical modulation of Cu-MOF-74 and the change of substance according to potential control. It was demonstrated that selective removal of $Cd^{2+}$ in aqueous solutions was feasible under a high concentration of co-existing $Na^{+}$. This study shows that the redox-active MOF assisted in the selective cation removal and subsequent electrosorbent regeneration, and demonstrates the feasibility of possible further development through organic linker modification or composite electrode formation.

## 2. Materials and methods

### 2.1. Materials

Cadmium chloride ($CdCl_2$), 2,5-dihydroxyterephthalic acid ($H_2$dobdc), copper nitrate hemi(pentahydrate) ($Cu(NO_3)_2{\cdot}2.5H_2O$), anhydrous N,N-dimethylformamide (DMF), and polyvinylpyrrolidone (PVDF) were purchased from Sigma Aldrich. Methyl alcohol (MeOH) and 2-propanol (IPA) were obtained from Junsei Chemical. All aqueous solutions were prepared using Milli-Q water (Millipore), and all chemicals were used without further purification.

### 2.2. Synthesis of Cu-MOF-74

Cu-based MOF-74 was synthesized according to the previously reported literature protocols [59]. In summary, 1.14 g of $CuNO_3{\cdot}2.5H_2O$ (4.9 mmol) and 0.44 g of $H_2$dobdc (2.24 mmol) were dissolved into a 50 mL mixture of DMF and IPA. The volume ratio between the solvents was 20:1 (DMF:IPA). The solution was heated to 100 °C for 18 h and then cooled slowly. The precipitate was recovered by vacuum filtration and washed with DMF. The dark-reddish MOF crystals were immersed in MeOH as an exchanging solvent for 24 h, replacing them with a fresh MeOH once during the solvent-exchange period. Finally, the products were dried in an oven at 80 °C under a vacuum for 24 h.

### 2.3. Electrochemically-assisted adsorption and desorption of $Cd^{2+}$

The electrode characterization and electrosorption performance of Cu-MOF-74 were analyzed by a Biologic potentiostat with a three-electrode configuration. To fabricate the working electrodes, a homogeneous slurry was prepared by mixing Cu-MOF-74 as an active material, carbon black (Super P; Alfa Aesar) as a conductive additive, and PVDF as a binder in a 8:1:1 wt ratio, respectively, and N-methyl-2-pyrrolidone (NMP) was used as a dispersant. The slurry was coated onto a stainless-steel mesh (325 mesh) as a base substrate (1 × 1 $cm^2$), and then dried in an oven at 80 °C under a vacuum overnight. The mass loading of the mixture was controlled to be 1 mg. As a control group, mesoporous carbon (Sigma Aldrich) and a Super P electrode were prepared separately in the same manner, using each as the active material. In the electrochemical experiments, Ag/AgCl and platinum wire were used as a reference electrode and a counter electrode, respectively. The volume of simulated wastewater or electrolyte was 10 mL unless otherwise noted. Before every electrosorption, the Cu-MOF-74 electrodes were electrochemically activated by conducting cyclic voltammetry in 0.1 mol $L^{-1}$ sodium perchlorate ($NaClO_4$) electrolyte in the range of −0.5 to 0.9 V (vs. Ag/AgCl) at a scan rate of 10 mV $s^{-1}$ for 3 cycles.

$Cd^{2+}$ containing solutions were prepared by adding a 0.1–100 mg $L^{-1}$ of $CdCl_2$ to the 20 mmol $L^{-1}$ NaCl aqueous solutions (pH 6.5). A simulated groundwater solution was prepared by dissolving chloride

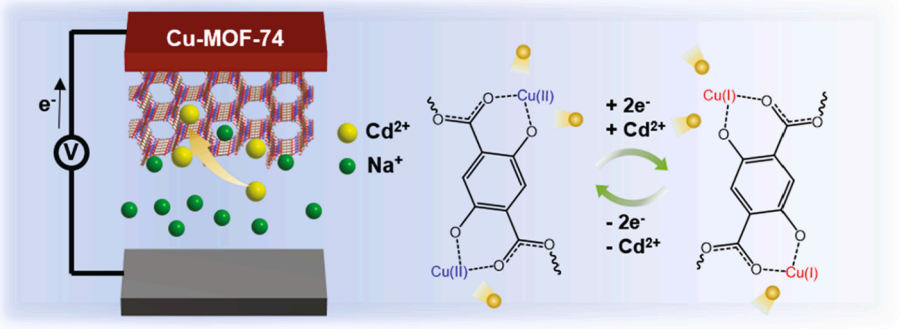


**Scheme 1.** Schematic representation of the electrochemically-assisted capture of cadmium ions.

salts containing 115 mg $L^{-1}$ $Na^+$, 180 mg $L^{-1}$ $K^+$, 110 mg $L^{-1}$ $Mg^{2+}$, and 25 mg $L^{-1}$ $Ca^{2+}$. For electrosorption and regeneration experiments, a constant potential with an appropriate value was applied onto a Cu-MOF-74 electrode with magnetic stirring at 250 rpm. To evaluate the selectivity for $Cd^{2+}$, we define the the separation factor ($SF_{Cd/Na}$), as can be calculated by the following equation:

$$SF_{Cd/Na} = \frac{Q_{Cd}/Q_{Na}}{C_{Cd,0}/C_{Na,0}} \quad (1)$$

where $Q_{Cd}$ and $Q_{Na}$ are the uptakes of $Cd^{2+}$ and $Na^+$, respectively, and $C_{Cd,0}$ and $C_{Na,0}$ are the initial concentrations of $Cd^{2+}$ and $Na^+$, respectively. $Cd^{2+}$ uptake kinetics was evaluated by applying −0.2 V (vs. Ag/AgCl) in 1 mmol $L^{-1}$ $CdCl_2$ + 20 mmol $L^{-1}$ NaCl for 10–120 min. The regeneration of Cu-MOF-74 was carried out with a 20 mmol $L^{-1}$ NaCl solution, and +0.9 V (vs. Ag/AgCl) was typically applied. The $Cd^{2+}$ or $Na^+$ concentrations were determined by inductively coupled plasma optical emission spectroscopy (ICP-OES 5110, Agilent), and the adsorption capacity of $Cd^{2+}$ was normalized by dividing it by the total mass loading on the electrodes.

The Coulombic efficiency (CE), which indicates the ratio of the amount of charge used for $Cd^{2+}$ adsorption to the amount of charge passed through the circuit, could be calculated through the following equation:

$$CE = \frac{n \times z \times F}{\int i dt} \times 100(\%) \quad (2)$$

where $n$ is the moles of adsorbed $Cd^{2+}$; $z$ is the number of involved electrons for adsorption of one $Cd^{2+}$ ion; $F$ is the Faraday constant; and $i$ is the current passed at time $t$. The z value was assumed to be 2 for the adsorption of divalent $Cd^{2+}$.

The specific energy (SE) consumption for the working electrode half-cell reaction was estimated through the following equation:

$$SE = \frac{\int_0^t E(t) i(t) dt}{m_{Cd}} \quad (3)$$

where $E(t)$ is the working electrode potential and $m_{Cd}$ is the adsorbed mass of Cd.

### 2.4. Physicochemical characterization

Morphological characterization and elemental analysis were carried out with a scanning electron microscope (SEM; SU5000, Hitachi) coupled with energy-dispersive spectroscopy (EDS) operated at an accelerating voltage of 5–15 kV. The porosity of Cu-MOF-74 was analyzed through the $N_2$ adsorption-desorption isotherm at 77 K, and the specific surface area was determined via a Brunauer-Emmett-Teller (BET) analysis (3Flex, Micrometrics). For pretreatment, the sample was degassed by heating to 180 °C for 6 h under a high vacuum. Fourier transform infrared (FT-IR; Nicolet iS50, Thermo) spectra were obtained in attenuated total reflectance (ATR) mode. Elemental survey and analysis of chemical states were conducted with X-ray photoelectron spectroscopy (XPS; K-alpha, Thermo) with a micro-focused monochromatic Al K(alpha) source (1486.7 eV). The XPS spectra were corrected with alkyl C 1 s reference (284.8 eV), and the analysis was carried out using Avantage software. X-ray diffraction patterns of the samples were obtained using an Ultima IV (Rigaku) with Cu Kα1 at a tube voltage of 45 kV and a current of 200 mA.

## 3. Results and discussion

### 3.1. Synthesis and characterization of Cu-MOF-74

The solvothermally-synthesized dark reddish Cu-MOF-74 powders were obtained as needle-shaped large crystals having a micron size width, as shown in SEM images (Fig. 1a and b). The highly crystalline phase can be confirmed through the PXRD analysis, and the pattern closely matched with the simulated PXRD pattern obtained from the literature (Fig. 1c) [59,60]. As shown in the FT-IR spectrum of Cu-MOF-74 (Fig. S1), the various peaks from the organic linker are consistent with the literature, and this confirmed that the solvent of DMF or methanol was well removed during the vacuum drying process, as previously reported [61]. To analyze the porosity and surface area, nitrogen adsorption/desorption isotherm at 77 K was obtained after the thermal pretreatment at 180 °C for 6 h under a high vacuum (Fig. 1d). It showed a typical Type I isotherm, which indicates a microporous structure, and the calculated BET specific surface area was 750 $m^2$ $g^{-1}$. The corresponding total pore volume at $P/P_o$ = 0.997 was 0.32 $cm^3$ $g^{-1}$, and it consisted mostly of micropores with pore widths under 1 nm.

### 3.2. Electrochemical removal of $Cd^{2+}$

The electrochemical behavior of the Cu-MOF-74 electrode was characterized through cyclic voltammetry (CV). Fig. 2a shows the typical initial few cycles of CV in 0.1 mol $L^{-1}$ of $NaClO_4$ aqueous solution at a scan rate of 10 mV $s^{-1}$. After the first activation cycle, each subsequent cycle showed a relatively stable curve shape, and it can be seen that the peak current slightly increased through the cycles. Three cycles of CV in a voltage window of −0.5 to +0.9 V (vs. Ag/AgCl) were conducted before the following electrosorption experiments to induce electrochemical activation. Based on the fifth cycle after stabilization in Fig. 2a, cathodic peaks were mainly observed at −0.09 and 0.06 V (vs. Ag/AgCl). From the electrochemical behaviors of Cu-based MOFs, it is believed that those peaks are assigned to the reduction of $Cu^{2+}$ or $Cu^+$ species existing in Cu-MOF-74, and the distinction between the two peaks is perhaps due to the redox of copper at different sites [56,62,63]. The corresponding anodic peaks can be observed at −0.07 and 0.21 V (vs. Ag/AgCl). A redox couple of an anodic peak at 0.35 V and a cathodic peak at 0.33 V (vs. Ag/AgCl) is possibly due to the redox in oxygen atoms [64].

Based on the observed redox-behavior of the Cu-MOF-74 electrode, we investigated the electrosorption of $Cd^{2+}$ in the range where electrodeposition of $Cd^{2+}$ ($E^0 \sim -0.6$ V vs. Ag/AgCl) is not expected to occur and the reduction of $Cu^{2+}$ or $Cu^+$ in the MOF crystal occurs. With a synthetic electrolyte solution containing 1 mmol $L^{-1}$ $CdCl_2$ and 20 mmol $L^{-1}$ NaCl, a constant potential was induced for 0.5 h to remove $Cd^{2+}$. As shown in Fig. 2b, the Cu-MOF-74 electrode could hardly remove $Cd^{2+}$ without electric potential (open-circuit voltage (O.C.) around +0.15 V vs. Ag/AgCl). In addition, an adsorption isotherm at 25 °C was obtained by dispersing and shaking the Cu-MOF-74 powder in various concentrations of $CdCl_2$ solutions (with a background of 20 mmol $L^{-1}$ NaCl) for 24 h, and this isotherm also showed low affinity of neutral Cu-MOF-74 to $Cd^{2+}$ (Fig. S2). Even when a weak potential of 0 V (vs. Ag/AgCl) was applied, it was not able to remove $Cd^{2+}$. However, when an overpotential of −0.1 V (vs. Ag/AgCl) or more negative overpotential was applied, the amount of $Cd^{2+}$ adsorbed increased as the negative voltage rose. The adsorbed $Cd^{2+}$ on the Cu-MOF-74 electrode can be seen in the SEM-EDS spectrum and elemental mapping images (Fig. S3). As a control group, carbon black electrodes (without Cu-MOF-74) and mesoporous carbon electrodes were tested at −0.3 V (vs. Ag/AgCl) for 0.5 h, but they showed low affinity toward $Cd^{2+}$ ions compared to the Cu-MOF-74 electrode (Fig. S4). From these results, the cathodic current according to the reduction of $Cu^{2+}$ attracted positively charged $Cd^{2+}$ ions effectively for electroneutrality.

### 3.3. Energy consumption analysis

Charge and energy consumption analyses were conducted to determine the appropriate potential for efficient electrosorption. First, Fig. 3a shows the calculated Coulombic efficiencies (Eq. (2)) after electrosorption for 0.5 h with the corresponding potentials applied, which were

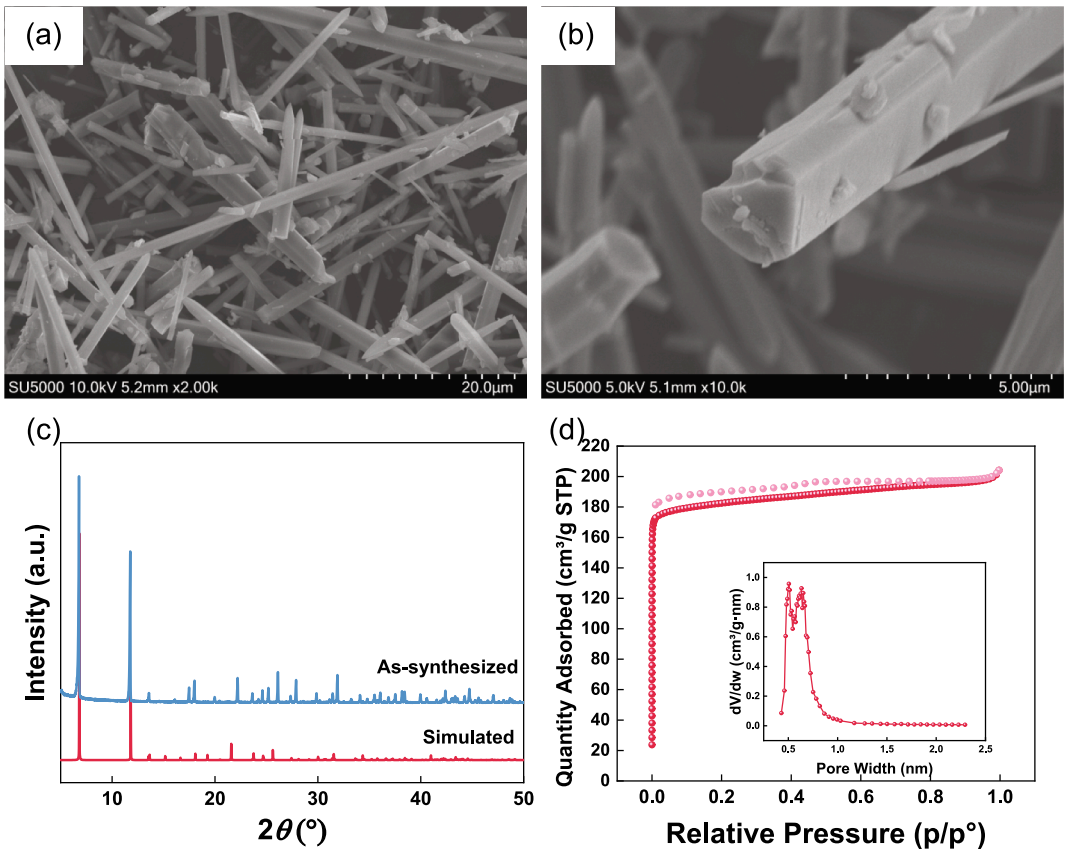


**Fig. 1.** (a) (b) SEM images and (c) XRD pattern of synthesized Cu-MOF-74. (d) Nitrogen adsorption-desorption isotherm of Cu-MOF-74 at 77 K and pore size distribution determined by Horvath-Kawazoe (HK) method (inset).

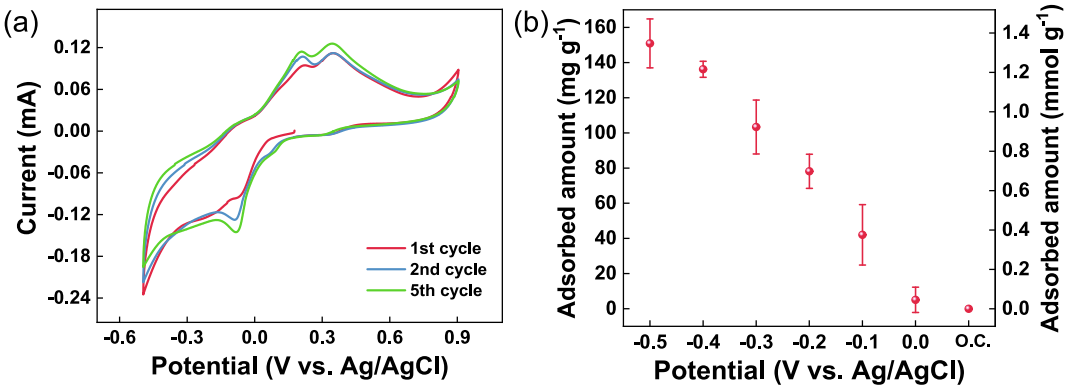


**Fig. 2.** (a) Cyclic voltammetry of Cu-MOF-74 electrode in the 0.1 mol $L^{-1}$ $NaClO_4$ electrolyte with a 10 mV $s^{-1}$ of scan rate and (b) electrosorption performance for $Cd^{2+}$ as a function of the working electrode (Cu-MOF-74) potential in the 1 mmol $L^{-1}$ $CdCl_2$ + 20 mmol $L^{-1}$ NaCl.

linked to the experiment in Fig. 2b. The amount of cadmium removal increased as the voltage increased in Fig. 2b, but the Coulombic efficiency gradually decreased. At the potentials of −0.2 to −0.3 V (vs. Ag/AgCl), Cu-MOF-74 exhibited similar efficiencies of around 45%, which was slightly higher than the efficiency of 42% for the mesoporous carbon. Meanwhile, from the same chronoamperometry experiment, the specific energy (SE) was estimated through the Eq. (3). As can be seen in Fig. 3b, the energy consumption used per mass of $Cd^{2+}$ adsorbed increased almost linearly with increasing voltage. The specific energy obtained at the adsorption potential of −0.3 V (vs. Ag/AgCl) was 11.0 kJ/g, which was slightly less than the value (17.0 kJ/g) in the case of mesoporous carbon with the same operational conditions. From these analyses, it can be seen that an effective $Cd^{2+}$ removal process utilizing the redox-activity of the Cu-MOF-74 electrode is feasible with high uptake capacity given the low specific energy consumption. In addition, −0.2 and −0.3 V (vs. Ag/AgCl) could be the most effective operating potentials considering the high electrosorption capacity with moderate energy and Faradaic efficiency, and therefore we focused on those potentials for the remaining experiments.

### 3.4. Electrosorption kinetics and selectivity

Electrosorption kinetics of $Cd^{2+}$ was evaluated at −0.2 V (vs. Ag/AgCl) in 1 mmol $L^{-1}$ $CdCl_2$ + 20 mmol $L^{-1}$ NaCl. As shown in Fig. 4a, the adsorption process on the Cu-MOF-74 electrode reached equilibrium after 0.5 h of operating time, showing rapid electrosorption kinetics and

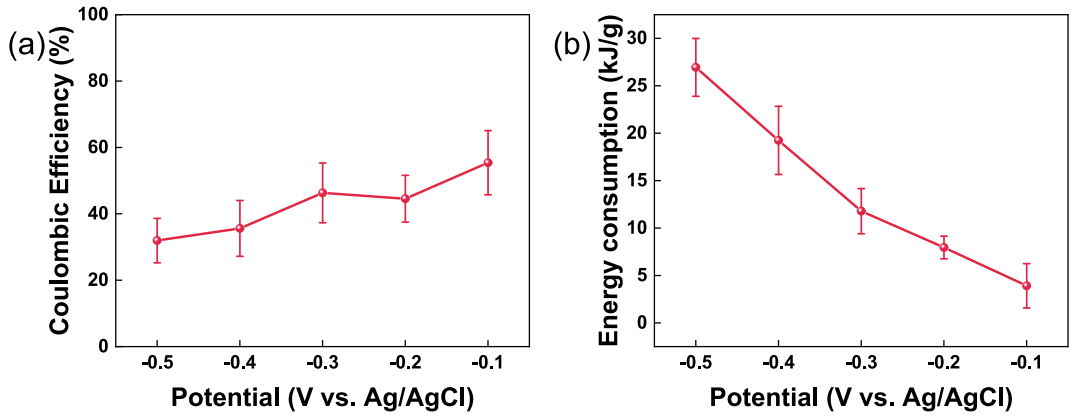


**Fig. 3.** (a) Coulombic efficiencies for $Cd^{2+}$ electrosorption and (b) specific energy consumption analysis results as a function of the working electrode potential in the 1 mmol $L^{-1}$ $CdCl_2$ + 20 mmol $L^{-1}$ NaCl electrolyte.

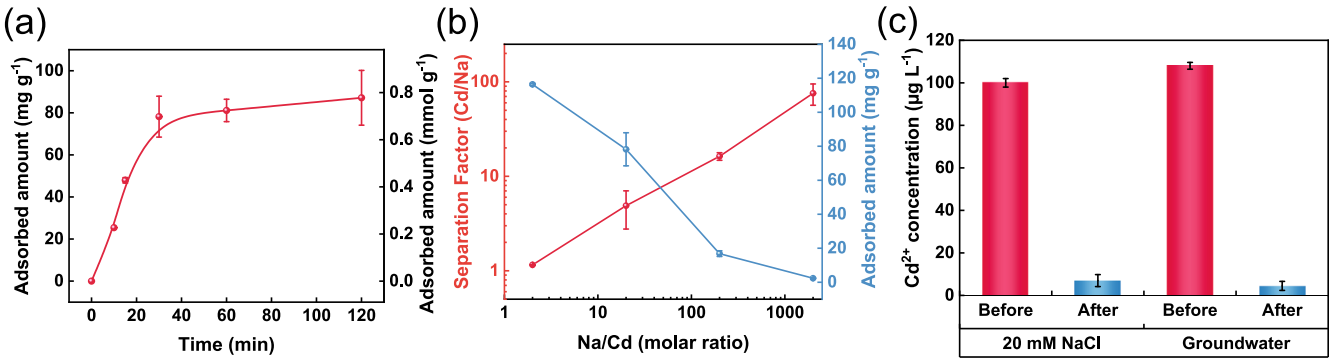


**Fig. 4.** (a) Electrosroption kinetics of Cu-MOF-74 electrodes in the 1 mmol $L^{-1}$ $CdCl_2$ + 20 mmol $L^{-1}$ NaCl with applied working electrode potentials of −0.2 V (vs. Ag/AgCl). (b) Electrosorption capacities and the separation factor (SF) with varying Na/Cd ratio (fixed NaCl concentration of 20 mmol $L^{-1}$) at −0.2 V (vs. Ag/AgCl) of working electrode potential. (c) Electrosorption of $Cd^{2+}$ in 20 mmol $L^{-1}$ NaCl and simulated groundwater solution at −0.2 V (vs. Ag/AgCl) of applied potential for 1 h.

affinity for $Cd^{2+}$. Given that no further increasing trend of $Cd^{2+}$ uptake was observed beyond equilibrium, reductive electrodeposition of $Cd^{2+}$ ions is not thought to be the mechanism of $Cd^{2+}$ removal, but rather it is assumed to be ion-binding onto electrostatically-charged sites. Based on these results, most of the electrosorption tests were carried out for 0.5–1 h.

Selective electrosorption performance was assessed by changing only the $CdCl_2$ concentration while the NaCl background salt concentration (20 mmol $L^{-1}$) was fixed. In addition, we chose to apply −0.2 V (vs. Ag/AgCl) for 0.5 h as operating conditions. The selectivity according to the Na/Cd molar ratios (2–2000) was evaluated using separation factor (Eq. (1)). As shown in Fig. 4b, the adsorbed amount of $Cd^{2+}$ of Cu-MOF-74 naturally decreased with increasing the Na/Cd ratio, and 116.4 mg $g^{-1}$ (1.04 mmol $g^{-1}$) high capacity was obtained in 10 mmol $L^{-1}$ $CdCl_2$ + 20 mmol $L^{-1}$ NaCl. On the contrary, the separation factor increased significantly with an increasing Na/Cd ratio, reaching 75 in $1 \times 10^{-2}$ mmol of $Cd^{2+}$. Furthermore, electrosorption tests for simulated wastewater containing low environmental concentrations of $Cd^{2+}$ (~1 μmol $L^{-1}$) were performed with 4 mL of solutions (Fig. 4c). As shown in Fig. 4c, in both 20 mmol $L^{-1}$ NaCl and simulated groundwater electrolyte (containing chloride salts of 115 mg $L^{-1}$ $Na^{+}$, 180 mg $L^{-1}$ $K^{+}$, 110 mg $L^{-1}$ $Mg^{2+}$, 25 mg $L^{-1}$ $Ca^{2+}$), over 93% of $Cd^{2+}$ could be removed by electrosorption at −0.2 V (vs. Ag/AgCl) only after an hour. These results almost met the 5 μg $L^{-1}$ of EPA drinking water standard. Therefore, it was shown that the Cd-MOF-74 electrode can selectively remove $Cd^{2+}$ even in the wastewater condition in which competitive $Na^{+}$ or other cations are dominantly dissolved.

### 3.5. Electrochemically-assisted regeneration and electrode stability

To investigate the electrochemically-mediated regenerability, +0.9 V (vs. Ag/AgCl) was applied to the Cd-adsorbed electrodes, which were previously reduced at −0.2 V (vs. Ag/AgCl) during electrosorption, in clean 20 mmol $L^{-1}$ NaCl electrolyte. Fig. 5a shows the regeneration kinetics of Cd-adsorbed Cu-MOF-74 electrodes. After 0.5 h of potential application, >50% of the adsorbed Cd was released into the aqueous phase, and the released amount of Cd increased with an almost linear trend. Significant amounts of adsorbed Cd were desorbed after 2 h of positive potential application, and finally the electrodes were almost fully regenerated. At this time, the amounts of copper released to the electrolyte over time were less than 1% of the mass of Cu-MOF-74 (Fig. S5). The regeneration of Cu-MOF-74 electrodes could also be confirmed in the ex-situ XPS survey (Fig. 5b). XPS peaks for Cd were newly observed in both a survey scan and Cd 3d narrow scan of the electrodes subjected to the adsorption process by negative potential (-0.2 V vs. Ag/AgCl for 1 h), whereas only small amounts of Cd remained in the electrodes that were regenerated by positive overpotential (+0.9 V vs. Ag/AgCl for 1.5 h). The same trend could be also confirmed in the SEM-EDS areal spectra (Fig. S6).

To validate the adsorption and desorption mechanism accompanied by the redox of copper in the Cu-MOF-74 structure, an ex-situ XPS Cu 2p narrow scan was carried out. As shown in Fig. 6a, the Cu $2p_{3/2}$ XPS spectrum of a pristine Cu-MOF-74 electrode could be deconvoluted into two peaks of $Cu^{+}$ centered at ~932.7 eV and $Cu^{2+}$ centered at ~935.0 eV, as in the literature [65]. The electrodes to which −0.1 and −0.2 V (vs. Ag/AgCl) were applied for 0.5 h also showed co-existence of the two

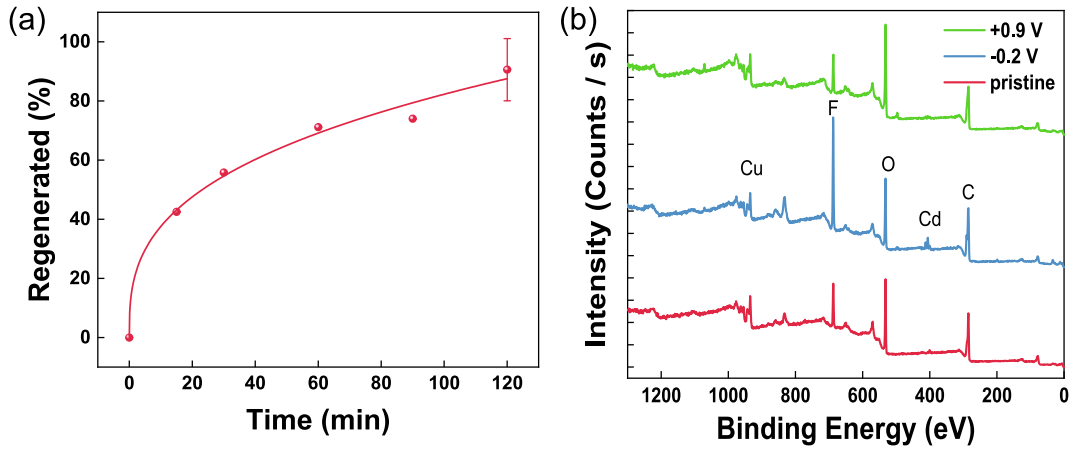


**Fig. 5.** (a) Regeneration kinetics of Cu-MOF-74 electrodes in the 20 mmol $L^{-1}$ NaCl at +0.9 V (vs. Ag/AgCl). Prior to the regeneration, electrosorption was conducted at −0.2 V (vs. Ag/AgCl) for 1 h. (b) XPS survey spectra of pristine Cu-MOF-74 electrode, after applying −0.2 V for 1 h in the electrolyte containing 1 mmol $L^{-1}$ $Cd^{2+}$, and after regeneration by applying +0.9 V for 1.5 h in clean NaCl electrolyte.

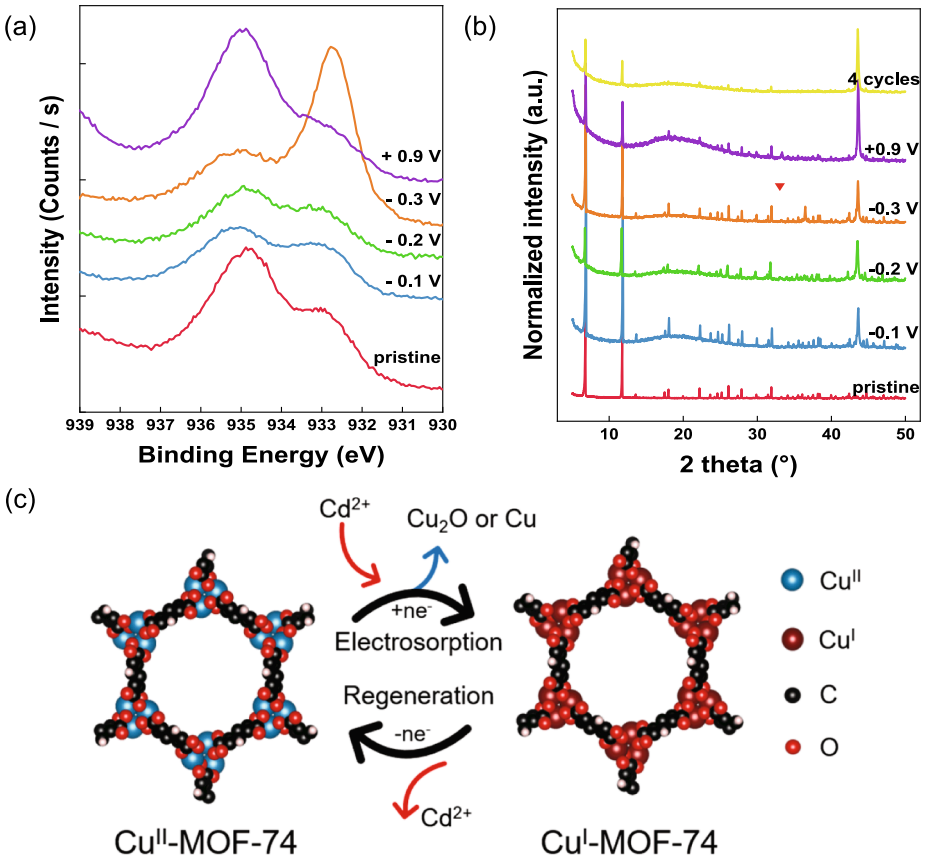


**Fig. 6.** (a) XPS Cu $2p_{1/3}$ spectra and (b) XRD patenrs of Cu-MOF-74 electrode as prepared, after electrosorption at −0.1, −0.2, and −0.3 V (vs. Ag/AgCl) for 0.5 h in 1 mmol $L^{-1}$ $CdCl_2$ + 20 mmol $L^{-1}$ NaCl, and after regeneration at +0.9 V (vs. Ag/AgCl) for 1.5 h 20 mmol $L^{-1}$ NaCl. Before the regeneration, −0.3 V (vs. Ag/AgCl) was applied in $CdCl_2$ containing solution for 0.5 h. Electrosorption/regeneration cycling was conducted at −0.2 V for 1 h and +0.9 V (vs. Ag/AgCl) for 2 h, respectively. Marked peak is related to cuprite ($Cu_2O$). (c) A schematic representation of the electrochemically-driven capture and release of $Cd^{2+}$ including $Cu_2O$ or $Cu^0$ formation.

oxidation states, but the ratio of the peak intensities corresponding to divalent to monovalent Cu decreased compared to the pristine electrode (Table S1). A ratio change between the two deconvoluted peaks was observed in a more dramatic manner for the electrode to which −0.3 V was applied. However, after the regeneration by applying +0.9 V (vs. Ag/AgCl) for 1.5 h to the electrode to which −0.3 V was applied for 0.5 h, it was confirmed that the peak area for $Cu^{2+}$ became larger again than that for $Cu^{+}$. From the XPS analysis, it was verified that the redox activity observed from the CV in Fig. 2a was due to the change in the oxidation state of the copper sites in Cu-MOF-74. In addition, it is expected that the redox activity of Cu could play a primary role in effective Cd removal and regeneration performance.

The stability in the crystal structure of the Cu-MOF-74 electrode after electrosorption of Cd or regeneration was evaluated through an ex-situ XRD analysis (Fig. 6b). In the XRD patterns corresponding to the electrode, unlike the powder sample, a peak located at 43.5° was observed due to the stainless-steel substrate (PDF#00-033-0397), and the ratio of the exposed area between the substrate and the coated material in the XRD specimen was not thoroughly controlled. The two main peaks located at 6.8° and 11.8°, which could be attributed to (1 1 0) and (3 0 0)

reflections from the Cu-MOF-74 crystal, respectively, were observed in all electrodes [59]. These results showed structural stability of the MOF after electrosorption or regeneration process. However, in the electrode to which −0.3 V (vs. Ag/AgCl) was applied, peaks at the 36.5° and 42.4° were newly generated, which were not clearly observed in the electrodes to which −0.1 V or −0.2 V was applied. These relatively broad peaks may correspond to cuprite, $Cu_2O$ crystal (PDF#01-073-6237), and the peaks could be removed after the regeneration process by applying +0.9 V (vs. Ag/AgCl), as confirmed by XRD and SEM (Fig. S7). Through the SEM observation, spherical particles could be observed on the surface, which were not found on the electrodes to which smaller potentials of −0.1 V and −0.2 V were applied. From the results of the EDS spot analysis, Cd was not detected in these spheres, unlike other surfaces, and it was confirmed that the spheres were mainly composed of copper. Moreover, it was estimated that the dramatic peak change in the XPS analysis results in Fig. 6a could be attributed to these particles, which were presumed to be $Cu_2O$ on the electrode surface. It is possible that overcharging can partially cause the formation of $Cu_2O$ or metallic Cu during the reduction process of Cu in Cu-MOF-74, and this effect may degrade the structural stability (Fig. 6c).

Based on these observations, −0.2 V (vs. Ag/AgCl) was set as the optimal operating potential to optimize the electrosorption capacity, Coulombic efficiency, energy efficiency, and structural stability. The electrosorption was conducted in 1 mmol $L^{-1}$ $CdCl_2$ + 20 mmol $L^{-1}$ NaCl solution for 1 h at −0.2 V (vs. Ag/AgCl), and the Cu-MOF-74 electrode was regenerated in 20 mM NaCl solution for 2 h at +0.9 V (vs. Ag/AgCl). Fig. 7 shows the adsorbed amount of Cd and the regeneration efficiency in each cycle after repeating the process four times. As a result, gradual degradation of sorption capacity was observed, which is presumed to be due to the occupied sorption sites after each incomplete regeneration, and the structural degradation observed in the XRD analysis also could affect this phenomenon. Nevertheless, high regeneration efficiency of over 80% was maintained in each cycle, and the adsorption capacity also could be kept above 60 mg $g^{-1}$ (0.54 mmol $g^{-1}$) without significant decay. This cycling result indicates that long-term operation can be feasible through sufficient optimization of operating conditions, and that Cu-MOF-74 could be an interesting material platform for further studies in Faradaic electrosorption processes.

## 4. Conclusions

We have demonstrated the redox-activity and capability of Cu-MOF-74 for effective cadmium removal and electrochemically-assisted regeneration. Through the use of a transition metal copper as a metal node in the MOF structure, the electrochemically-assisted adsorption and desorption of $Cd^{2+}$ ions were induced by the redox reaction on the copper node. We investigated the effect of the cathodic current generated by the reduction of divalent copper to monovalent copper on the large amount of adsorbed $Cd^{2+}$ (>0.9 mmol $g^{-1}$) in an energy-efficient manner. In addition, the Cu-MOF-74 electrode was able to selectively uptake $Cd^{2+}$ against a high concentration of $Na^+$. Conversely, the copper reduced during the electrosorption of cadmium was oxidized to divalent copper by positive overpotential, and the Cu-MOF-74 electrode could be completely regenerated. As a result of morphological and structural analyses according to the electrochemical process, it was observed that applying overly high overpotential over −0.3 V (vs. Ag/AgCl) could promote a side reaction of $Cu_2O$ formation. Consequently, the optimal operating conditions were explored to address material stability, energy-efficiency, and adsorption capacity, and it was shown that stable electrosorption and regeneration was possible for four cycles. Thus, we demonstrate that target ions such as Cd in this study in wastewater can be effectively and selectively removed by utilizing the redox-activity of the metal nodes in the MOFs. In addition, it is expected that the work in this study can show the feasibility of employing redox-active MOFs in electrochemical wastewater treatment, and with potential redox-behaviors incorporated in a variety of metal sties and organic linkers in the future, enhancing stability and molecular selectivity.

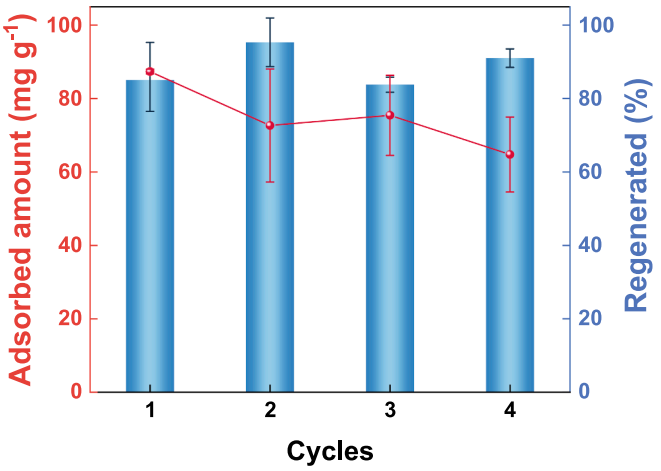


**Fig. 7.** Cycling performance of Cu-MOF-74 electrode. The electrosorption was conducted at −0.2 V (vs. Ag/AgCl) for 1 h in the 1 mmol $L^{-1}$ $CdCl_2$ + 20 mmol $L^{-1}$ NaCl, and +0.9 V (vs. Ag/AgCl) was applied for 2 h in the 20 mmol $L^{-1}$ NaCl for the regeneration.

## Declaration of Competing Interest

The authors declare that they have no known competing financial interests or personal relationships that could have appeared to influence the work reported in this paper.

## Acknowledgements

The authors are grateful for the financial support from the UK-Republic of Korea Joint Research Program through the NRF grant (NRF-2019M2A7A1001773) funded by the Ministry of Science and ICT, Republic of Korea. X. Su and K. Kim thank U.S. Department of Energy, Office of Basic Energy Sciences, for support based on Award Number DOE DE-SC0021409.

## Appendix A. Supplementary data

Supplementary data to this article can be found online at https://doi.org/10.1016/j.cej.2021.129765.

## References

[1] V. Pothanamkandathil, J. Fortunato, C.A. Gorski, Electrochemical desalination using intercalating electrode materials: a comparison of energy demands, Environ. Sci. Technol. 54 (2020) 3653–3662, https://doi.org/10.1021/acs.est.9b07311.
[2] Q. Li, Y. Zheng, D. Xiao, T. Or, R. Gao, Z. Li, M. Feng, L. Shui, G. Zhou, X. Wang, Z. Chen, Faradaic electrodes open a new era for capacitive deionization, Adv. Sci. 7 (2020) 2002213, https://doi.org/10.1002/advs.202002213.
[3] Y.K. Kim, T. Kim, Y. Kim, D. Harbottle, J.W. Lee, Highly effective Cs + removal by turbidity-free potassium copper hexacyanoferrate-immobilized magnetic hydrogels, J. Hazard. Mater. 340 (2017) 130–139, https://doi.org/10.1016/j.jhazmat.2017.06.066.
[4] D.-H. Nam, D. Lee, K.-S. Choi, Electrochemical and photoelectrochemical approaches for the selective removal, recovery, and valorization of chloride ions, Chem. Eng. J. 404 (2020), 126378, https://doi.org/10.1016/j.cej.2020.126378.
[5] P. Srimuk, J. Lee, A. Tolosa, C. Kim, M. Aslan, V. Presser, Titanium disulfide: a promising low-dimensional electrode material for sodium ion intercalation for seawater desalination, Chem. Mater. 29 (2017) 9964–9973, https://doi.org/10.1021/acs.chemmater.7b03363.
[6] X. Tang, Q. Li, Z. Wang, Y. Hu, Y. Hu, R. Li, In situ electrokinetic isolation of cadmium from paddy soil through pore water drainage: effects of voltage gradient and soil moisture, Chem. Eng. J. 337 (2018) 210–219, https://doi.org/10.1016/j.cej.2017.12.111.
[7] Q. Peng, L. Liu, Y. Luo, Y. Zhang, W. Tan, F. Liu, S.L. Suib, G. Qiu, Cadmium removal from aqueous solution by a deionization supercapacitor with a birnessite electrode, ACS Appl. Mater. Interfaces 8 (2016) 34405–34413, https://doi.org/10.1021/acsami.6b12224.

[8] H.H. Kyaw, M.T.Z. Myint, S. Al-Harthi, M. Al-Abri, Removal of heavy metal ions by capacitive deionization: effect of surface modification on ions adsorption, J. Hazard. Mater. (2019), 121565, https://doi.org/10.1016/j.jhazmat.2019.121565.

[9] D. Purkayastha, U. Mishra, S. Biswas, A comprehensive review on Cd(II) removal from aqueous solution, J. Water Process Eng. 2 (2014) 105–128, https://doi.org/10.1016/j.jwpe.2014.05.009.

[10] C.-H. Huang, L. Chen, C.-L. Yang, Effect of anions on electrochemical coagulation for cadmium removal, Sep. Purif. Technol. 65 (2009) 137–146, https://doi.org/10.1016/j.seppur.2008.10.029.

[11] F. Fu, Q. Wang, Removal of heavy metal ions from wastewaters: a review, J. Environ. Manage. 92 (2011) 407–418, https://doi.org/10.1016/j.jenvman.2010.11.011.

[12] L.R. Rad, A. Momeni, B.F. Ghazani, M. Irani, M. Mahmoudi, B. Noghreh, Removal of Ni2+and Cd2+ions from aqueous solutions using electrospun PVA/zeolite nanofibrous adsorbent, Chem. Eng. J. 256 (2014) 119–127, https://doi.org/10.1016/j.cej.2014.06.066.

[13] W. Liu, D. Wang, R.A. Soomro, F. Fu, N. Qiao, Y. Yu, R. Wang, B. Xu, Ceramic supported attapulgite-graphene oxide composite membrane for efficient removal of heavy metal contamination, J. Memb. Sci. 591 (2019), 117323, https://doi.org/10.1016/j.memsci.2019.117323.

[14] Y. Kim, H.H. Eom, D. Kim, D. Harbottle, J.W. Lee, Adsorptive removal of cesium by electrospun nanofibers embedded with potassium copper hexacyanoferrate, Sep. Purif. Technol. 255 (2021), 117745, https://doi.org/10.1016/j.seppur.2020.117745.

[15] Y.K. Kim, S. Kim, Y. Kim, K. Bae, D. Harbottle, J.W. Lee, Facile one-pot synthesis of dual-cation incorporated titanosilicate and its deposition to membrane surfaces for simultaneous removal of Cs+ and Sr2+, Appl. Surf. Sci. 493 (2019) 165–176, https://doi.org/10.1016/j.apsusc.2019.07.008.

[16] J.Y. Yoon, H. Zhang, Y.K. Kim, D. Harbottle, J.W. Lee, A high-strength polyvinyl alcohol hydrogel membrane crosslinked by sulfosuccinic acid for strontium removal via filtration, J. Environ. Chem. Eng. 7 (2019), 102824, https://doi.org/10.1016/j.jece.2018.102824.

[17] C. Li, Y. Yan, Q. Zhang, Z. Zhang, L. Huang, J. Zhang, Y. Xiong, S. Tan, Adsorption of Cd 2+ and Ni 2+ from aqueous single-metal solutions on graphene oxide-chitosan-poly(vinyl alcohol) hydrogels, Langmuir 35 (2019) 4481–4490, https://doi.org/10.1021/acs.langmuir.8b04189.

[18] Y. Kim, Y.K. Kim, S. Kim, D. Harbottle, J.W. Lee, Nanostructured potassium copper hexacyanoferrate-cellulose hydrogel for selective and rapid cesium adsorption, Chem. Eng. J. 313 (2017) 1042–1050, https://doi.org/10.1016/j.cej.2016.10.136.

[19] J.E. Efome, D. Rana, T. Matsuura, C.Q. Lan, Metal-organic frameworks supported on nanofibers to remove heavy metals, J. Mater. Chem. A 6 (2018) 4550–4555, https://doi.org/10.1039/c7ta10428f.

[20] H. Zhang, S. Tangparitkul, B. Hendry, J. Harper, Y.K. Kim, T.N. Hunter, J.W. Lee, D. Harbottle, Selective separation of cesium contaminated clays from pristine clays by flotation, Chem. Eng. J. 355 (2019) 797–804, https://doi.org/10.1016/j.cej.2018.07.135.

[21] H. Zhang, C.S. Hodges, P.K. Mishra, J.Y. Yoon, T.N. Hunter, J.W. Lee, D. Harbottle, Bio-inspired preparation of clay-hexacyanoferrate composite hydrogels as super adsorbents for Cs +, ACS Appl. Mater. Interfaces 12 (2020) 33173–33185, https://doi.org/10.1021/acsami.0c06598.

[22] D. Sarma, S.M. Islam, K.S. Subrahmanyam, M.G. Kanatzidis, Efficient and selective heavy metal sequestration from water by using layered sulfide $K_{2x}Sn_{4-x}S_{8-x}$ (x = 0.65–1; KTS-3), J. Mater. Chem. A 4 (2016) 16597–16605, https://doi.org/10.1039/C6TA06404C.

[23] S. Deng, G. Zhang, S. Liang, P. Wang, Microwave assisted preparation of thio-functionalized polyacrylonitrile fiber for the selective and enhanced adsorption of mercury and cadmium from water, ACS Sustain. Chem. Eng. 5 (2017) 6054–6063, https://doi.org/10.1021/acssuschemeng.7b00917.

[24] K. Kim, P. Baldaguez Medina, J. Elbert, E. Kayiwa, R.D. Cusick, Y. Men, X. Su, Molecular tuning of redox-copolymers for selective electrochemical remediation, Adv. Funct. Mater. (2020) 2004635, https://doi.org/10.1002/adfm.202004635.

[25] X. Du, H. Zhang, X. Hao, G. Guan, A. Abudula, Facile preparation of ion-imprinted composite film for selective electrochemical removal of nickel(II) ions, ACS Appl. Mater. Interfaces 6 (2014) 9543–9549, https://doi.org/10.1021/am501926u.

[26] R. Chen, T. Sheehan, J.L. Ng, M. Brucks, X. Su, Capacitive deionization and electrosorption for heavy metal removal, Environ. Sci. Water Res. Technol. 6 (2020) 258–282, https://doi.org/10.1039/c9ew00945k.

[27] M.E. Suss, S. Porada, X. Sun, P.M. Biesheuvel, J. Yoon, V. Presser, Water desalination via capacitive deionization: what is it and what can we expect from it? Energy Environ. Sci. 8 (2015) 2296–2319, https://doi.org/10.1039/c5ee00519a.

[28] X. Yang, L. Liu, W. Tan, G. Qiu, F. Liu, High-performance Cu2+ adsorption of birnessite using electrochemically controlled redox reactions, J. Hazard. Mater. 354 (2018) 107–115, https://doi.org/10.1016/j.jhazmat.2018.04.069.

[29] L. Xu, C. Yu, Y. Mao, Y. Zong, B. Zhang, H. Chu, D. Wu, Can flow-electrode capacitive deionization become a new in-situ soil remediation technology for heavy metal removal? J. Hazard. Mater. 402 (2021), 123568 https://doi.org/10.1016/j.jhazmat.2020.123568.

[30] E.N. Guyes, T. Malka, M.E. Suss, Enhancing the ion-size-based selectivity of capacitive deionization electrodes, Environ. Sci. Technol. 53 (2019) 8447–8454, https://doi.org/10.1021/acs.est.8b06954.

[31] X. Su, K.J. Tan, J. Elbert, C. Rüttiger, M. Gallei, T.F. Jamison, T.A. Hatton, Asymmetric Faradaic systems for selective electrochemical separations, Energy Environ. Sci. 10 (2017) 1272–1283, https://doi.org/10.1039/c7ee00066a.

[32] K. Singh, L. Zhang, H. Zuilhof, L.C.P.M. de Smet, Water desalination with nickel hexacyanoferrate electrodes in capacitive deionization: experiment, model and comparison with carbon, Desalination 496 (2020), 114647, https://doi.org/10.1016/j.desal.2020.114647.

[33] X. Su, T.A. Hatton, Electrosorption at functional interfaces: from molecular-level interactions to electrochemical cell design, Phys. Chem. Chem. Phys. 19 (2017) 23570–23584, https://doi.org/10.1039/c7cp02822a.

[34] K. Tang, Y. ha Kim, J. Chang, R.T. Mayes, J. Gabitto, S. Yiacoumi, C. Tsouris, Seawater desalination by over-potential membrane capacitive deionization: opportunities and hurdles, Chem. Eng. J. 357 (2019) 103–111. https://doi.org/10.1016/j.cej.2018.09.121.

[35] Y. Cho, K.S. Lee, S.C. Yang, J. Choi, H.R. Park, D.K. Kim, A novel three-dimensional desalination system utilizing honeycomb-shaped lattice structures for flow-electrode capacitive deionization, Energy Environ. Sci. 10 (2017) 1746–1750, https://doi.org/10.1039/c7ee00698e.

[36] N. Kim, X. Su, C. Kim, Electrochemical lithium recovery system through the simultaneous lithium enrichment via sustainable redox reaction, Chem. Eng. J. (2020), 127715, https://doi.org/10.1016/j.cej.2020.127715.

[37] X. Zhang, K. Zuo, X. Zhang, C. Zhang, P. Liang, Selective ion separation by capacitive deionization (CDI) based technologies: a state-of-the-art review, Environ. Sci. Water Res. Technol. 6 (2020) 243–257, https://doi.org/10.1039/C9EW00835G.

[38] X. Su, T.A. Hatton, Redox-electrodes for selective electrochemical separations, Adv. Colloid Interface Sci. 244 (2017) 6–20, https://doi.org/10.1016/j.cis.2016.09.001.

[39] X. Su, Electrochemical interfaces for chemical and biomolecular separations, Curr. Opin. Colloid Interface Sci. 46 (2020) 77–93, https://doi.org/10.1016/j.cocis.2020.04.005.

[40] P. Srimuk, X. Su, J. Yoon, D. Aurbach, V. Presser, Charge-transfer materials for electrochemical water desalination, ion separation and the recovery of elements, Nat. Rev. Mater. 5 (2020) 517–538, https://doi.org/10.1038/s41578-020-0193-1.

[41] C. Choi, D.S. Ashby, D.M. Butts, R.H. DeBlock, Q. Wei, J. Lau, B. Dunn, Achieving high energy density and high power density with pseudocapacitive materials, Nat. Rev. Mater. 5 (2020) 5–19, https://doi.org/10.1038/s41578-019-0142-z.

[42] K. Kim, S. Cotty, J. Elbert, R. Chen, C. Hou, X. Su, Asymmetric redox-polymer interfaces for electrochemical reactive separations: synergistic capture and conversion of arsenic, Adv. Mater. 32 (2020) 1906877, https://doi.org/10.1002/adma.201906877.

[43] X. Su, A. Kushima, C. Halliday, J. Zhou, J. Li, T.A. Hatton, Electrochemically-mediated selective capture of heavy metal chromium and arsenic oxyanions from water, Nat. Commun. 9 (2018) 4701, https://doi.org/10.1038/s41467-018-07159-0.

[44] R. Candeago, K. Kim, H. Vapnik, S. Cotty, M. Aubin, S. Berensmeier, A. Kushima, X. Su, Semiconducting polymer interfaces for electrochemically assisted mercury remediation, ACS Appl. Mater. Interfaces 12 (2020) 49713–49722, https://doi.org/10.1021/acsami.0c15570.

[45] T. Islamoglu, Z. Chen, M.C. Wasson, C.T. Buru, K.O. Kirlikovali, U. Afrin, M. R. Mian, O.K. Farha, Metal-organic frameworks against toxic chemicals, Chem. Rev. 120 (2020) 8130–8160, https://doi.org/10.1021/acs.chemrev.9b00828.

[46] F. Ke, L.-G. Qiu, Y.-P. Yuan, F.-M. Peng, X. Jiang, A.-J. Xie, Y.-H. Shen, J.-F. Zhu, Thiol-functionalization of metal-organic framework by a facile coordination-based postsynthetic strategy and enhanced removal of Hg2+ from water, J. Hazard. Mater. 196 (2011) 36–43, https://doi.org/10.1016/J.JHAZMAT.2011.08.069.

[47] L. Mendecki, K.A. Mirica, Conductive metal-organic frameworks as ion-to-electron transducers in potentiometric sensors, ACS Appl. Mater. Interfaces 10 (2018) 19248–19257, https://doi.org/10.1021/acsami.8b03956.

[48] M. Ko, L. Mendecki, K.A. Mirica, Conductive two-dimensional metal-organic frameworks as multifunctional materials, Chem. Commun. 54 (2018) 7873–7891, https://doi.org/10.1039/c8cc02871k.

[49] M. Feng, P. Zhang, H.C. Zhou, V.K. Sharma, Water-stable metal-organic frameworks for aqueous removal of heavy metals and radionuclides: a review, Chemosphere 209 (2018) 783–800, https://doi.org/10.1016/j.chemosphere.2018.06.114.

[50] C. Wang, X. Liu, N. Keser Demir, J.P. Chen, K. Li, Applications of water stable metal-organic frameworks, Chem. Soc. Rev. 45 (2016) 5107–5134, https://doi.org/10.1039/c6cs00362a.

[51] L.S. Xie, G. Skorupskii, M. Dincă, Electrically conductive metal-organic frameworks, Chem. Rev. 120 (2020) 8536–8580, https://doi.org/10.1021/acs.chemrev.9b00766.

[52] X. Deng, J.-Y. Hu, J. Luo, W.-M. Liao, J. He, Conductive metal-organic frameworks: mechanisms, design strategies and recent advances, Top. Curr. Chem. 378 (2020) 27, https://doi.org/10.1007/s41061-020-0289-5.

[53] J. Calbo, M.J. Golomb, A. Walsh, Redox-active metal-organic frameworks for energy conversion and storage, J. Mater. Chem. A 7 (2019) 16571–16597, https://doi.org/10.1039/c9ta04680a.

[54] J.H. Park, H. Kim, M. Kim, J.M. Lim, J. Ryu, S. Kim, Sequential removal of radioactive Cs by electrochemical adsorption and desorption reaction using core-shell structured carbon nanofiber–Prussian blue composites, Chem. Eng. J. 399 (2020), 125817, https://doi.org/10.1016/j.cej.2020.125817.

[55] Y. Zheng, J. Qiao, J. Yuan, J. Shen, A. jun Wang, L. Niu, Electrochemical removal of radioactive cesium from nuclear waste using the dendritic copper hexacyanoferrate/carbon nanotube hybrids, Electrochim. Acta 257 (2017) 172–180. https://doi.org/10.1016/j.electacta.2017.09.179.

[56] P. Wang, X. Du, T. Chen, X. Hao, A. Abudula, K. Tang, G. Guan, A novel electroactive PPy/HKUST-1 composite film-coated electrode for the selective recovery of lithium ions with low concentrations in aqueous solutions, Electrochim. Acta 306 (2019) 35–44, https://doi.org/10.1016/j.electacta.2019.03.106.

[57] I. Choi, Y.E. Jung, S.J. Yoo, J.Y. Kim, H.J. Kim, C.Y. Lee, J.H. Jang, Facile synthesis of M-MOF-74 (M=Co, Ni, Zn) and its application as an electrocatalyst for electrochemical CO2 conversion and H2 production, J. Electrochem. Sci. Technol. 8 (2017) 61–68, https://doi.org/10.5229/JECST.2017.8.1.61.

[58] X. Su, L. Bromberg, V. Martis, F. Simeon, A. Huq, T.A. Hatton, Postsynthetic functionalization of Mg-MOF-74 with tetraethylenepentamine: structural characterization and enhanced CO2 adsorption, ACS Appl. Mater. Interfaces 9 (2017) 11299–11306, https://doi.org/10.1021/acsami.7b02471.

[59] R. Sanz, F. Martínez, G. Orcajo, L. Wojtas, D. Briones, Synthesis of a honeycomb-like Cu-based metal-organic framework and its carbon dioxide adsorption behaviour, Dalton Trans. 42 (2013) 2392–2398, https://doi.org/10.1039/c2dt32138f.

[60] P. Leo, G. Orcajo, D. Briones, G. Calleja, M. Sánchez-Sánchez, F. Martínez, A recyclable Cu-MOF-74 catalyst for the ligand-free O-arylation reaction of 4-nitrobenzaldehyde and phenol, Nanomaterials 7 (2017) 149, https://doi.org/10.3390/nano7060149.

[61] J.G. Flores, E. Sánchez-González, A. Gutiérrez-Alejandre, J. Aguilar-Pliego, A. Martínez, T. Jurado-Vázquez, E. Lima, E. González-Zamora, M. Díaz-García, M. Sánchez-Sánchez, I.A. Ibarra, Greener synthesis of Cu-MOF-74 and its catalytic use for the generation of vanillin, Dalton Trans. 47 (2018) 4639–4645, https://doi.org/10.1039/c7dt04701k.

[62] S.D. Worrall, M.A. Bissett, W. Hirunpinyopas, M.P. Attfield, R.A.W. Dryfe, Facile fabrication of metal-organic framework HKUST-1-based rewritable data storage devices, J. Mater. Chem. C 4 (2016) 8687–8695, https://doi.org/10.1039/c6tc03496a.

[63] R. Senthil Kumar, S. Senthil Kumar, M. Anbu Kulandainathan, Highly selective electrochemical reduction of carbon dioxide using Cu based metal organic framework as an electrocatalyst, Electrochem. Commun. 25 (2012) 70–73, https://doi.org/10.1016/j.elecom.2012.09.018.

[64] Q. Jiang, P. Xiong, J. Liu, Z. Xie, Q. Wang, X.Q. Yang, E. Hu, Y. Cao, J. Sun, Y. Xu, L. Chen, A redox-active 2D metal-organic framework for efficient lithium storage with extraordinary high capacity, Angew. Chem. Int. Ed. 59 (2020) 5273–5277, https://doi.org/10.1002/anie.201914395.

[65] A.K. Adhikari, K.S. Lin, Synthesis, fine structural characterization, and CO2 adsorption capacity of metal organic frameworks-74, J. Nanosci. Nanotechnol. 14 (2014) 2709–2717, https://doi.org/10.1166/jnn.2014.8621.